HD^+ photodissociation in the scaled coordinate approach

Vladimir Roudnev* and B. D. Esry†
Department of Physics and J.R. Macdonald Laboratory, Kansas State University, Manhattan, Kansas 66506, USA
(Received 31 August 2004; published 18 January 2005)

The scaled coordinate approach is applied to the problem of HD^+ photodissociation in a short, intense, infrared laser pulse. Two- and three-dimensional models for the molecule aligned in the field of a linearly polarized laser are studied. Scaling allows substantial improvements in the numerical accuracy and provides a simple way to calculate the fragments' energy spectra.

DOI: 10.1103/PhysRevA.71.013411 PACS number(s): 33.80.Gj, 42.50.Hz, 33.80.Wz, 33.80.Eh

I. INTRODUCTION

The numerical solution of the time-dependent Schrödinger equation remains the main tool for investigation of few-body systems in short intense laser pulses [1–3]. One common problem, though, with time-dependent approaches is that they are necessarily limited to a finite integration volume: when part of the physical system reaches the boundary, artifacts due to reflections appear. This problem is often solved via absorbing boundary conditions by introducing an imaginary potential or masking function. Such boundary conditions, however, lead to lost information. Numerical solutions are further complicated by a phase that accumulates rapidly with time and distance, making the wave function oscillate rapidly. These oscillations make numerical approximation of the wave function difficult, especially when long propagation times are required.

A coordinate scaling technique that addresses both of these problems was proposed in Ref. [5] as an adaptation of the ideas in Ref. [4], and one-dimensional (1D) tests of the technique were reported in Ref. [6]. This technique combines coordinate and wave function transformations that localize continuum wave packets in space and essentially eliminates growing spatial oscillations. By analytically eliminating these purely kinematic effects, the wave function can more easily be propagated to larger times. The ability to propagate the wave function longer is essential for calculating the velocity distributions of the final state: the propagation must be long enough that the final state fragments no longer interact significantly with each other. Another useful feature of the scaled coordinate method is a straightforward way to extract the velocity distribution from the final state density function, the wave function itself is not required. Further, knowledge of the density function in the whole configuration space is not necessary, as all coordinates corresponding to the internal degrees of freedom of the final state fragments can be integrated out. Taken together, these features make the scaled coordinate approach extremely useful for treating systems in several dimensions.

The aim of this work is to demonstrate how the scaled coordinate approach works in practical calculations of molecular dissociation. We demonstrate that the momentum distribution can be extracted directly from the scaled coordinate density function, discuss improved numerical accuracy provided by the method, and apply it to two- and three-dimensional models of HD^+ photodisintegration.

II. SCALED COORDINATE APPROACH AND ITS PROPERTIES

In this section we provide a brief introduction to the scaled coordinate approach and demonstrate some important large-time properties of the wave function in scaled coordinates.

Consider a particle of mass m in a one-dimensional space described by a coordinate x and acted upon by an external potential $V(x,t)$. The wave function satisfies the time-dependent Schrödinger equation (TDSE) in atomic units,

$$i\frac{\partial}{\partial t}\Psi(x,t)=\left[-\frac{1}{2m}\frac{\partial^2}{\partial x^2}+V(x,t)\right]\Psi(x,t). \tag{1}$$

The scaled coordinate approach amounts to a time-dependent change of variables,

$$x=R(t)\xi \tag{2}$$

plus a wave function transformation,

$$\Psi^S(\xi,t)=\sqrt{R}e^{-i(m/2)R\dot{R}\xi^2}\Psi(R\xi,t), \tag{3}$$

where the dot indicates the time derivative. The scaled wave function Ψ^S satisfies the following modified Schrödinger equation:

$$i\frac{\partial}{\partial t}\Psi^S(\xi,t)=\left[-\frac{1}{2mR^2}\frac{\partial^2}{\partial \xi^2}+V(R\xi,t)+\frac{1}{2}mR\ddot{R}\xi^2\right]\Psi^S(\xi,t). \tag{4}$$

This equation has been obtained by many authors in various contexts [4,7–9]. In these cases, though, the scaling function R was chosen as a physical quantity in the system, or to facilitate an approximate solution. In our case we use R to facilitate the numerical—but otherwise exact—solution. For instance, in Ref. [4] and subsequent developments [10–13] that treat the problem of ion-atom scattering, the scaling factor R was taken to be the distance between nuclei which were treated classically. As discussed in Ref. [5], however, R need not correspond to a physical quantity and can be chosen to have any convenient form.

Equation (4) costs little more to solve numerically than the original equation (1). It has, however, two properties that

*Electronic address: roudnev@phys.ksu.edu
†Electronic address: esry@phys.ksu.edu

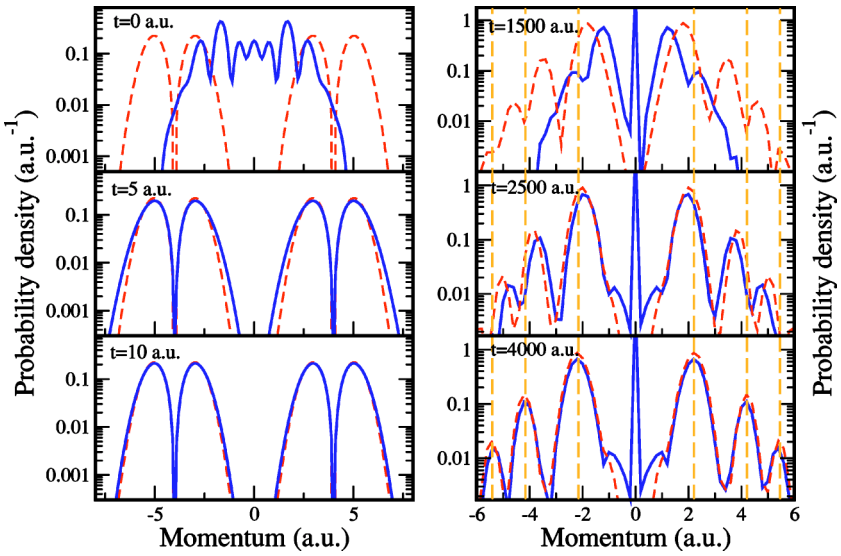

FIG. 1. (Color online) Momentum distributions calculated from a Fourier transform (dashed lines) and from the scaled coordinate density function (solid lines). The left panel shows free particle evolution; and the right, photodetachment of a particle bound with a short-range potential. The scaling parameter is $v_x=1.414$ for the free particle case and 9.759×10^{-3} for the photodetachment model, making convergence of scaled spatial distribution to the momentum distribution much faster for the free particle.

must be taken into account: an extra time-dependent potential $\frac{1}{2}mR\ddot{R}\xi^2$ and bound states that shrink as R grows. The impact of both factors can be minimized by choosing the second derivative of the scaling function $R(t)$ to be smooth enough to avoid introducing an extra, unphysical time scale. In practice, a good choice is

$$R(t)=\begin{cases}1\ , t<t_0\\ [1+v_x^4(t-t_0)^4]^{1/4}\ , t\geqslant t_0\end{cases}, \tag{5}$$

where v_x is the asymptotic scaling coefficient and has units of velocity, while t_0 is the scaling start time. This function has a continuous second derivative, which switches the extra potential term on smoothly. The shrinking bound states can be handled using nonuniform grids that are denser in the appropriate regions of configuration space.

At large times, the scaling function behaves like $R(t)\rightarrow v_xt$, which insures some important asymptotic properties for Ψ^S. As was shown in Ref. [6], for instance, the scaled wave function does not oscillate as strongly as the original one, making it easier to approximate numerically. In particular, it was shown that at large times a Gaussian wave packet becomes stationary in the scaled coordinates. Here we sketch a generalization of this result.

To this end, consider the momentum representation for the wave function,

$$\tilde{\Psi}(p,t)=\frac{1}{\sqrt{2\pi}}\int_{-\infty}^{\infty}dx e^{-ipx}\Psi(x,t). \tag{6}$$

Using the relationship between the scaled and unscaled coordinate representations for the wave function (3), evaluating the integral (6) in the stationary phase approximation [16], and assuming $R(t)\approx v_xt$, we find the following expression for the momentum representation:

$$\tilde{\Psi}(p,t)=e^{-i(\pi/4)}\frac{1}{\sqrt{mv_x}}e^{i(p^2/2m)t}\Psi^S\left(\frac{p}{mv_x},t\right)+O((mv_x^2t)^{-3/2}). \tag{7}$$

This formula demonstrates that for infinite propagation time the wave function in scaled coordinates becomes stationary, approaching the momentum space wave function up to a phase. The kinetic factor $e^{i(p^2/2m)t}$ includes all the explicit time dependence of the wave function in momentum space, hence the scaled wave function is stationary.

In fact, the scaling method has played no critical role in this result since Ψ^S is related to the usual lab-frame wave function by a simple transformation. Physically, we are doing nothing more than using time of flight to calculate the momentum distribution. What the scaling method does is to make numerical time propagation to very large times a tractable prospect. It is thus possible to obtain the momentum distribution directly from the scaled coordinate wave function without performing a Fourier transform. A similar observation was made in Refs. [12–15]. In particular, combining our expressions (7) and (3) gives Eq. (48) from Ref. [15].

Equation (7) also suggests that the convergence of the scaled wave function to its stationary form depends on the asymptotic scaling coefficient v_x so that the faster $R(t)$ grows, the faster the density distribution in scaled coordinates converges to the momentum density distribution. These observations are illustrated in Fig. 1 by two test cases: a free propagation of some initial state (left column) and a toy model of a charged massive ($m=150\ m_e$) particle bound in a short-range potential experiencing a short intense laser pulse (right column). The momentum distributions calculated at different propagation times are shown together with the corresponding distributions obtained from the scaled wave function using Eq. (7). For the free particle case (Fig. 1, left column), the initial spatial distribution is indicated by the solid lines for $t=0$ and the mean velocity is zero. Since there are no bound states, there are no limitations on v_x. We can thus choose a large value to guarantee fast convergence of the scaled distribution to the momentum distribution. In the

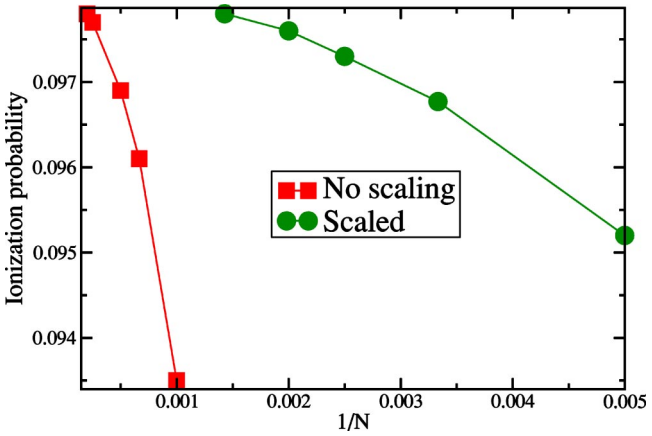

FIG. 2. (Color online) Convergence of the ionization probability for a model system with respect to the number of grid points N. The solid line shows the scaled results and the dashed line the unscaled results.

second case (Fig. 1, right column), the short-range potential supports only one bound state. The system is then exposed to a short intense laser pulse in closer analogy to the present situation of molecular photodissociation. The scaling function and grid must satisfy several conditions: (i) the grid must accurately represent the bound state throughout the whole propagation; (ii) the propagation time must be long enough to stabilize the final state momentum distribution such that the dissociated fragments feel no force due to the short range potential; and (iii) the scaling start time must be chosen to keep the whole wave function contained within the grid. For illustration purposes, we have chosen the potential and laser parameters such that the corresponding spatial and temporal scales are comparable to the HD^+ photodissociation case. Further, we chose the laser parameters so that the multiphoton absorption structure of the momentum distribution could be clearly seen. The well-distinguishable maxima at $p=\pm 2.2, \pm 4.2$, and ± 5.5 a.u. in the resulting distribution correspond to one-, two-, and three-photon absorption, respectively. We have also seen that the time required to obtain a stable momentum distribution from a Fourier transform is comparable to the time required for convergence of the scaled coordinate distribution to the distribution in momentum space.

The scaled coordinate approach provides other important numerical advantages as well. Besides making continuum wave packets stationary in space, the scaled coordinate approach insures that the number of nodes in the real or imaginary parts of the wave function is about the same as the number of peaks in the corresponding density function. Such a function is more easily approximated numerically than the original wave function [which strongly oscillates in space due to the $e^{i(1/2)mR\dot{R}\xi^2}$ factor in the Eq. (3)], since fewer nodes require fewer points to represent the wave function to a given accuracy. To demonstrate this fact, we solved the TDSE using a three-point finite difference scheme [17] and operator-splitting with Cayley approximations to the exponential operators. The results are presented in Fig. 2, showing the convergence of the ionization probability for the model of a massive particle bound with a short-range potential in a short laser pulse. It is seen that the scaled results converge much faster, requiring more than five times fewer grid points than without scaling to achieve the same accuracy. Another important feature of the scaled coordinate approach is that the longer propagation times needed to achieve sufficient final state channel separation do not require denser spatial grids. As mentioned in Ref. [5], the only factor that limits the propagation time is the presence of bound states since the bound states in scaled coordinates shrink with time. This problem can be solved, however, by using nonuniform grids more dense in the regions where the bound states are localized. In practice, we employ a grid with points distributed as $x_i \propto i^3$ near the origin to handle the bound states that smoothly transition to $x_i \propto i$ at large distances as is appropriate for free propagation.

III. SCALED COORDINATE APPROACH FOR HD^+ IN A LASER FIELD

Although the scaled coordinate approach is very effective when applied to atomic ionization, it is not so obvious that it will also have advantages for treating general molecular dissociation. The primary complication is the complex structure of configuration space due to the presence of so multiple centers. In contrast to atomic ionization, molecular dissociation involves both atomic and molecular bound states which are localized in different regions of configuration space.

A. 2D model

The utility of scaled coordinates for HD^+ dissociation can be readily demonstrated using a 2D model. In this model, the motion of both the electron and the nuclei are restricted to one dimension, z and R, respectively, assumed to be along the laser polarization. Such a model describes both ionization and dissociation processes. The time evolution of the three-particle system is thus described by the Schrödinger equation

$$i\frac{\partial}{\partial t}\Psi = [H_0 + W(t)]\Psi. \tag{8}$$

In this equation H_0 is the field-free Hamiltonian [20]

$$H_0 = -\frac{1}{2\mu_{pd}}\frac{\partial^2}{\partial R^2} - \frac{1}{2\mu_e}\frac{\partial^2}{\partial z^2} - \frac{1}{\sqrt{(z-z_p)^2 + a(R)}} - \frac{1}{\sqrt{(z+z_d)^2 + a(R)}} + \frac{1}{R}, \tag{9}$$

where $z_p=[m_d/(m_p+m_d)]R$ and $z_d=[m_p/(m_p+m_d)]R$ are the positions of the proton and deuteron, m_p and m_d are the proton and deuteron masses, and μ_{pd} and μ_e are the reduced masses,

$$\frac{1}{\mu_{pd}} = \frac{1}{m_p} + \frac{1}{m_d} \text{ and } \frac{1}{\mu_e} = 1 + \frac{1}{m_p + m_d}. \tag{10}$$

As is usual in reduced dimensions, the Coulomb potentials are softened. To make the model more realistic, we vary the parameter a with the internuclear distance to reproduce the

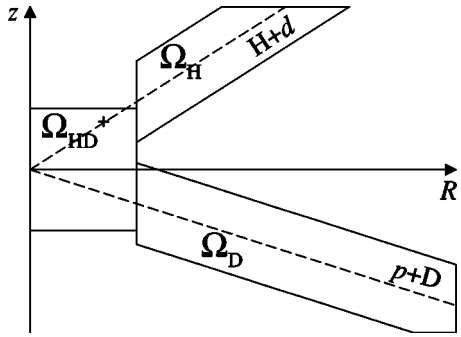

FIG. 3. Domains in configuration space corresponding to different final states. The asymmetry of the domains is due to the nuclear mass difference: H fragments move faster than D fragments with respect to the center of mass.

$1\sigma_g$ Born-Oppenheimer potential curve. The interaction with the laser is (in the length gauge)

$$W(t) = E(t)\left[\frac{m_d - m_p}{m_p + m_d}R - \frac{m_p + m_d + 2}{m_p + m_d + 1}z\right], \tag{11}$$

in which the electric field $E(t)$ has a Gaussian envelope

$$E(t) = E_0 e^{-(t/\tau)^2}\cos(\omega t + \phi). \tag{12}$$

In this expression, τ is the pulse duration, ω is the carrier frequency of the laser, ϕ is the carrier-envelope phase difference (CEPD), and E_0 is the pulse amplitude in atomic units. In our calculations we take $\tau = 248$ a.u., corresponding to a 10-fs full width at half maximum (FWHM) pulse, and carrier frequencies of $\omega = 0.058$ a.u. and $\omega = 0.1$ a.u.

Even though it is simple, the two-dimensional model allows us to investigate the applicability of the scaling approach to photodissociation processes. As mentioned above, in contrast to atomic ionization, the dynamics of nuclei in a molecule generate much richer physics. The configuration space of the 2D model is shown in Fig. 3. The bound states of the molecule are localized in the region labeled Ω_{HD^+} near the coordinate origin. The two-body subsystems, i.e., hydrogen and deuterium atoms, are localized in the infinite domains Ω_H and Ω_D. When scaling is applied to the electronic and nuclear coordinates, these domains start to shrink, making the corresponding dissociation channels more difficult to reproduce numerically.

Another practical problem comes from the dynamics of an electron in the field of an intense infrared laser. For laser intensities around 10^{15} W/cm^2, the classical electron quiver amplitude is about 100 a.u. The combined requirements of covering this range in the electronic coordinate, accurately reproducing the atomic channels, and representing the fast oscillations of the wave function in the electronic coordinate induced by the interaction with the laser field lead to unreasonably large electronic grids. For instance, tests with a 1D model suggest that about 3000 grid points are required to obtain a numerically stable final state for the ionization channel. In this work, we concentrate our attention on dissociation only, and allow the ionized electrons to be absorbed in the boundary region by an optical potential. Since we do not have to keep the free electrons in the final state and the grid

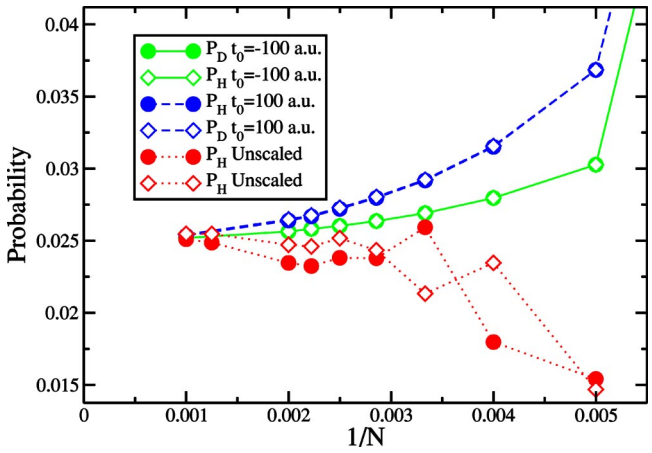

FIG. 4. (Color online) Convergence of the dissociation probability in the 2D model. P_H is the probability to dissociate to H+d; and P_D, to p+D.

in the electronic coordinate already contains the quiver motion of the electron, we apply scaling to the internuclear distance R only.

The results of convergence tests for HD^+ ground state photodissociation at the intensity 7×10^{14} W/cm^2, laser frequency $\omega = 0.058$ a.u., and 10-fs FWHM long pulse are shown in Fig. 4. There we plot the probabilities of ground state dissociation to each of the channels versus the inverse number of grid points in the nuclear coordinate. Solid and dashed lines correspond to the scaled calculations, and the dotted lines reflect the results obtained without scaling. The two scaled calculations differ by the scaling start time. The three-point finite difference scheme that we employ [17] is expected to converge at the rate $O(N^{-3})$, where N is the number of grid points in the internuclear distance R. Obviously, both scaled sets converge more smoothly than the unscaled one. Further, the scaled results demonstrate the smooth convergence for a much wider range of grid sizes, whereas the unscaled results can be considered smooth and monotonic only when the number of grid points is more than 500 at best. It is also clear that the scaling start time is an important parameter influencing the convergence rate. For the earlier start time, the numerical error of the scaled calculations is more than two times smaller than the error of unscaled calculations performed on a grid of the same number of points, even though the scaling is turned on before the peak field of the laser.

It is instructive to compare these 2D dissociation probabilities with those from a 3D model [18]. The 2D model is able to qualitatively reproduce some properties obtained in the 3D calculations. For instance, the prediction that the maximum dissociation probability is observed for a peak intensity around $I = 7\times10^{14}$ W/cm^2 (Fig. 5) is reproduced. To some extent, CEPD effects can also been observed within the 2D model (Fig. 6), although the magnitude of the effect is not as big as predicted in three dimensions. In fact, only scaling allowed us to reduce the numerical error sufficiently to see the small CEPD effect within the 2D model. Quantitative comparison, however, shows that the ground state dissociation probabilities calculated with the 2D model are underestimated by about ten times with respect to more realistic

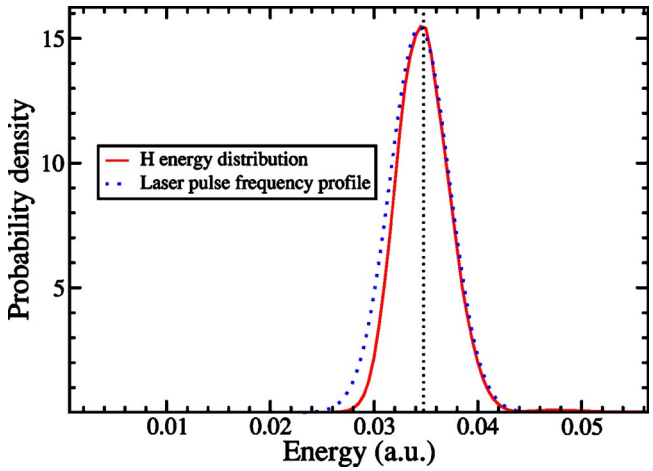

FIG. 5. (Color online) Kinetic energy distribution of the dissociated fragments in the center of mass frame for a 2D model of H_2^+. The eighth excited state was exposed to a laser pulse of 10 fs FWHM, $I=10^{12}$ W/cm^2, and $\omega=0.1$ a.u. The vertical dotted line shows the position of the peak expected from energy conservation.

3D calculations, consistent with the calculations of Ref. [19].

The relationship (7) provides a simple way to recover the velocity distribution from the scaled density function. To demonstrate this point, we show in Fig. 7 the dissociation probability in the perturbative regime for a 2D model of H_2^+ in a 10-fs FWHM laser pulse with $\omega=0.1$ a.u and a peak intensity of 1×10^{12} W/cm^2. The initial state is chosen as the eighth vibrationally excited state ($v=8$) with an energy $E_8=-0.53$ a.u. These parameters were chosen to produce an easily recognized energy distribution for one-photon absorption in the perturbative regime. One photon absorption produces a distinctive peak around the fragment energy $(E_8-E_H+\omega)/2$, where $E_H=-0.5$ a.u. is the energy of the hydrogen atom ground state. As expected, the peak profile closely follows the laser pulse frequency profile. The small deviations from the exact laser frequency profile can be attributed to nonlinear processes which do contribute even at a peak intensity as low as 1×10^{12} W/cm^2.

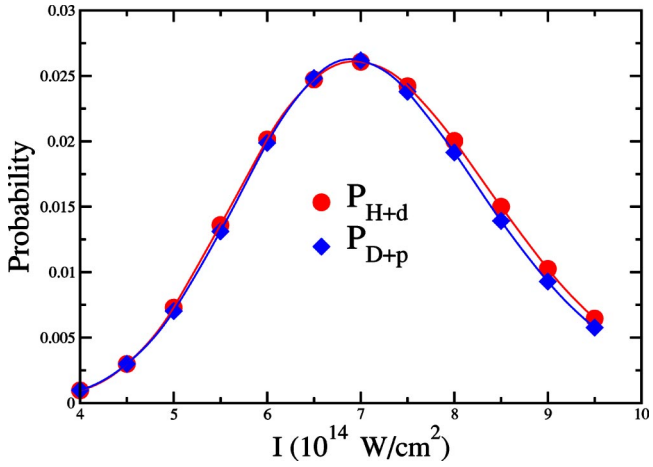

FIG. 6. (Color online) Intensity dependence of the HD+ (2D model) dissociation probability in the field of 10-fs FWHM, 785-nm laser pulse.

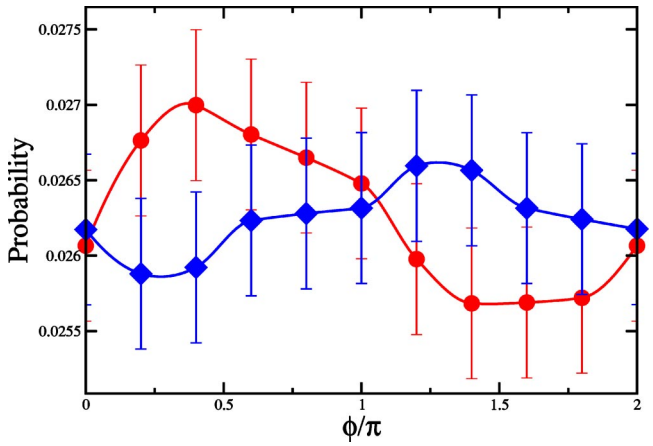

FIG. 7. (Color online) Carrier-envelope phase dependence of the HD+ (2D model) dissociation probability in the field of 10-fs FWHM, 785-nm laser pulse with peak intensity $I=7\times10^{14}$ W/cm^2. The error bars are estimated from convergence tests like those shown in Fig. 4.

B. 3D model

A more realistic approach allows the electron two degrees of freedom, corresponding to the assumption that the nuclei are aligned with the linearly polarized laser and not allowed to rotate. Considering initial σ electronic states, the azimuthal electron coordinate can be eliminated by symmetry. The six-dimensional configuration space is thus reduced to three dimensional [2,20,21]: (R,ρ,z), where R is the internuclear distance and (ρ,z) are the cylindrical coordinates of the electron. In this case the operator H_0 in Eq. (8) reads

$$H_0=-\frac{1}{2\mu_{pd}}\frac{\partial^2}{\partial R^2}-\frac{1}{2\mu_e}\left(\frac{\partial^2}{\partial\rho^2}+\frac{1}{\rho}\frac{\partial}{\partial\rho}+\frac{\partial^2}{\partial z^2}\right)-\frac{1}{\sqrt{(z-z_p)^2+\rho^2}}-\frac{1}{\sqrt{(z+z_d)^2+\rho^2}}+\frac{1}{R}. \quad (13)$$

As in the 2D model, we apply scaling to the internuclear distance only. Compared to our previous unscaled calculations [18], scaling has allowed us to improve the number of points in the nuclear coordinate by a factor of 2 while keeping the error constant. The representation of states with large nuclear separation could then be improved, yielding a precision about two times better overall (Fig. 8).

The fragment velocity distribution obtained from the scaled coordinate density function is presented in Fig. 9. The fragment center of mass frame velocities are reconstructed from the scaled density function of the final time using momentum conservation. Channel selection is performed via integrating the density function in electronic coordinates over the appropriate regions of configuration space (Fig. 3). The difference in the fragments' velocity distributions for the different dissociation channels is clearly seen. Although the structure of the velocity spectrum for a molecule dissociated by an ultrashort laser pulse is the subject for separate research, we can emphasize one important feature of the velocity distribution. As was mentioned in Ref. [18] and shown in Fig. 8, the probability of dissociation is expected to demonstrate clearly observable spatial asymmetry resulting from

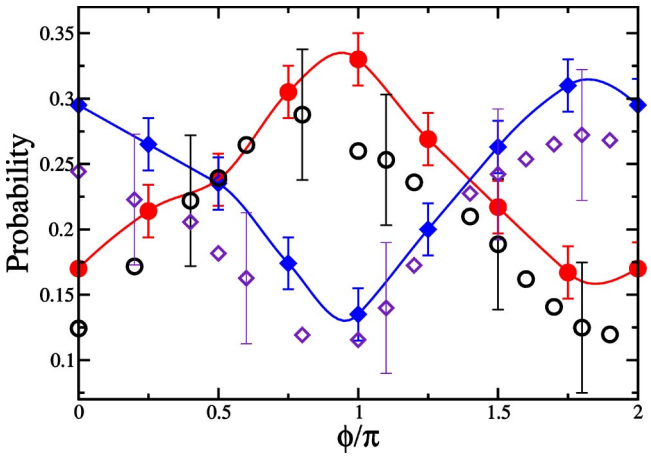

FIG. 8. (Color online) Carrier-envelope phase dependence of the HD^+ dissociation probability in the field of 10-fs FWHM, 785-nm laser pulse with peak intensity $I=7\times10^{14}$ W/cm^2, 3D model. The open symbols denote our previous [18] unscaled results (circles for P_H and diamonds for P_D). The filled symbols denote the present scaled results (circles for P_H and diamonds for P_D).

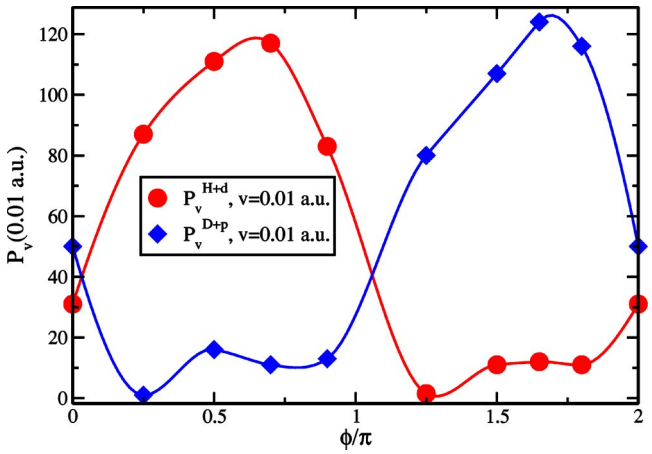

FIG. 10. (Color online) Dissociation of the HD^+ ground state in 10-fs, 785-nm laser pulse with peak intensity $I=7\times10^{14}$ W/cm^2: CEPD dependence of the probability density at the fragment relative velocity 0.01 a.u.

CEPD effects if channel selection is performed. Even stronger effects could be observed if channel selection is supplemented with fragment velocity selection, as can be concluded from Fig. 10. There we present the laser phase dependence of the velocity-selected probability density. The total dissociation signal measured along the polarization direction varies by a factor of 3 depending on the laser phase (Fig. 8), whereas the variation of a velocity-selected signal covers a range of 1–100 (Fig. 10). Such sharp velocity selectivity is not possible experimentally, but we expect that the strong enhancement should survive inclusion of experimental resolution.

IV. SUMMARY

Techniques for the numerical solution of the time-dependent Schrödinger equation are of fundamental importance for the physics of short laser pulses interacting with molecules. As was mentioned in Ref. [6], two fundamental problems of wave function time propagation are solved by the scaled coordinate approach: the translation and spreading of free wave packets, which necessitate large grids, and the wave function phase rapidly growing in space and time, which requires dense grids or limited propagation times. The scaling technique explicitly eliminates both problems without any serious numerical complications. The scaled Schrödinger equation is nearly as easy to solve as the original one, but with fewer constraints for the grid and propagation time. The only limitation for time propagation is the ability to reproduce bound states. For systems with a single center, such as atoms, this problem can be easily solved using nonuniform grids; multicenter molecular systems are more difficult to treat. Their subsystems' bound states are distributed over infinite domains in at least one coordinate, making them difficult to cover with a sufficiently dense grid. Even so, applying the scaled coordinate method to only some of the coordinates still leads to important computational savings. Our error estimate for the dissociation probability of the HD^+ in a 10-fs infrared laser pulse has, for instance, been halved compared to our previous unscaled calculations. At the same time, the scaling technique provides an efficient way to extract fragment velocity distributions from a partial density function integrated over all but the relative coordinates of the dissociated fragments. This quantity is much easier to manipulate than the wave function in the whole configuration space, which would be required when calculating the velocity distributions with other techniques.

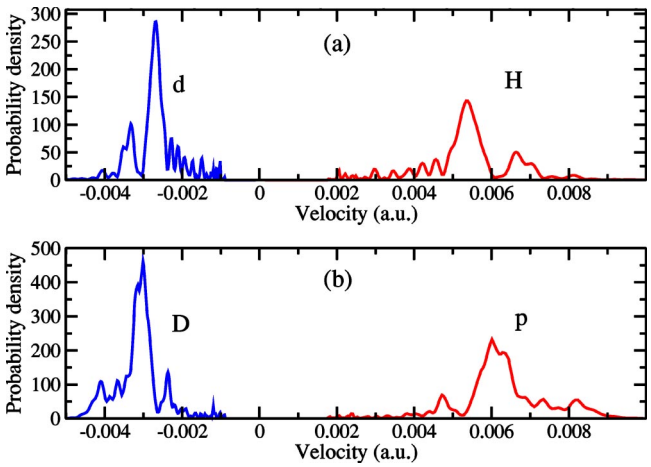

FIG. 9. (Color online) Velocity distributions of the fragments in the center-of-mass frame after dissociation of the HD^+ ground state in 10-fs, 785-nm laser pulse with peak intensity $I=7\times10^{14}$ W/cm^2: (a) $H+d$ channel and (b) $p+D$ channel.

ACKNOWLEDGMENT

This work was supported by the Chemical Sciences, Geosciences, and Biosciences Division, Office of Basic Energy Sciences, Office of Science, U.S. Department of Energy.

[1] A. D. Bandrauk and S. Chelkowski, Phys. Rev. Lett. **84**, 3562 (2000).
[2] D. Dundas, K. J. Meharg, J. F. McCann, and K. T. Taylor, Eur. Phys. J. D **26**, 51 (2003).
[3] B. Feuerstein and U. Thumm, Phys. Rev. A **67**, 043405 (2003).
[4] E. A. Soloviev and S. I. Vinitsky, J. Phys. B **18**, L557 (1985).
[5] E. Y. Sidky and B. D. Esry, Phys. Rev. Lett. **85**, 5086 (2000).
[6] Z. X. Zhao, B. D. Esry, and C. D. Lin, Phys. Rev. A **65**, 023402 (2002).
[7] Y. Kagan, E. L. Surkov, and G. V. Shlyapnikov, Phys. Rev. A **54**, R1753 (1996); **55**, R18 (1997).
[8] Y. Castin and R. Dum, Phys. Rev. Lett. **77**, 5315 (1996).
[9] G. M. Bruun and C. W. Clark, Phys. Rev. A **61**, 061601(R) (2000).
[10] T. P. Grozdanov and E. A. Solov'ev, Phys. Rev. A **44**, 5605 (1991).
[11] S. Yu. Ovchinnikov and J. H. Macek, Phys. Rev. Lett. **75**, 2474 (1995).
[12] J. H. Macek and S. Yu. Ovchinnikov, Phys. Rev. Lett. **80**, 2298 (1998).
[13] S. Yu. Ovchinnikov, G. N. Ogurtsov, J. H. Macek, and Yu. S. Gordeev, Phys. Rep. **389**, 119 (2004).
[14] M. Daumer *et al.*, J. Stat. Phys. **88**, 967 (1997).
[15] V. N. Serov, A. Keller, O. Atabek, and N. Billy, Phys. Rev. A **68**, 053401 (2003).
[16] V. P. Maslov and M. V. Fedoriuk, *Semi-Classical Approximation in Quantum Mechanics* (D. Reidel, Dordrecht, 1981).
[17] M. W. J. Bromley and B. D. Esry, Phys. Rev. A **69**, 053620 (2004).
[18] V. Roudnev, B. D. Esry, and I. Ben-Itzhak, Phys. Rev. Lett. **93**, 163601 (2004).
[19] G. L. Ver Steeg, K. Bartschat, and I. Bray, J. Phys. B **36**, 3325 (2003).
[20] S. Chelkowski, A. Conjusteau, T. Zuo, and A. D. Bandrauk, Phys. Rev. A **54**, 3235 (1996).
[21] I. Kawata, H. Kono, and Y. Fujimura, J. Chem. Phys. **110**, 11 152 (1999).